

PCCP

Accepted Manuscript



This is an *Accepted Manuscript*, which has been through the Royal Society of Chemistry peer review process and has been accepted for publication.

Accepted Manuscripts are published online shortly after acceptance, before technical editing, formatting and proof reading. Using this free service, authors can make their results available to the community, in citable form, before we publish the edited article. We will replace this *Accepted Manuscript* with the edited and formatted *Advance Article* as soon as it is available.

You can find more information about *Accepted Manuscripts* in the [Information for Authors](#).

Please note that technical editing may introduce minor changes to the text and/or graphics, which may alter content. The journal's standard [Terms & Conditions](#) and the [Ethical guidelines](#) still apply. In no event shall the Royal Society of Chemistry be held responsible for any errors or omissions in this *Accepted Manuscript* or any consequences arising from the use of any information it contains.

**Reaction Rate Constants of H-Abstraction by OH from Large Ketones:
Measurements and Site-Specific Rate Rules**

Jihad Badra^{1,2}, Ahmed Elwardany¹, Aamir Farooq^{1,*}

¹Clean Combustion Research Center, Division of Physical Sciences and Engineering, King Abdullah University of Science and Technology (KAUST), Thuwal 23955, Saudi Arabia

²Saudi Aramco Research and Development Center, Fuel Technology R&D Division, Dhahran 31311, Saudi Arabia

*Corresponding Author - Email: aamir.farooq@kaust.edu.sa, Phone: +966128082704

Abstract

Reaction rate constants for the reaction of four large ketones with hydroxyl (OH) are investigated behind reflected shock waves using OH laser absorption. The studied ketones are isomers of hexanone and include 2-hexanone, 3-hexanone, 3-methyl-2-pentanone, and 4-methyl-2-pentanone. Rate constants are measured under pseudo-first-order kinetics at temperatures ranging from 866 K to 1375 K and pressures near 1.5 atm. The reported high-temperature rate constant measurements are the first direct measurements for these ketones at combustion-relevant conditions. The effects of the position of the carbonyl group (C=O) and methyl (CH₃) branching on the overall rate constant with OH are examined. Using previously published data, rate constant expressions covering low-to-high temperatures are developed for acetone, 2-butanone, 3-pentanone, and the hexanone isomers studied here. These Arrhenius expressions are used to devise rate rules for H-abstraction from various sites. Specifically, the current scheme is applied with good success to H-abstraction by OH from a series of *n*-ketones. Finally, general expressions for primary and secondary site-specific H-abstraction by OH from ketones are proposed as follows (the subscripts numbers indicate the number of carbon atoms bonded to the next-nearest-neighbor carbon atom, the subscript CO indicates that the abstraction is from a site next to the carbonyl group (C=O), and the prime is used to differentiate different neighboring environments of a methylene group):

$$P_{1,CO} = 7.38 \times 10^{-14} \exp(-274 \text{ K}/T) + 9.17 \times 10^{-12} \exp(-2499 \text{ K}/T) \quad (285 - 1355 \text{ K})$$

$$S_{10,CO} = 1.20 \times 10^{-11} \exp(-2046 \text{ K}/T) + 2.20 \times 10^{-13} \exp(160 \text{ K}/T) \quad (222 - 1464 \text{ K})$$

$$S_{11,CO} = 4.50 \times 10^{-11} \exp(-3000 \text{ K}/T) + 8.50 \times 10^{-15} \exp(1440 \text{ K}/T) \quad (248 - 1302 \text{ K})$$

$$S_{11',CO} = 3.80 \times 10^{-11} \exp(-2500 \text{ K}/T) + 8.50 \times 10^{-15} \exp(1550 \text{ K}/T) \quad (263 - 1370 \text{ K})$$

$$S_{21,CO} = 5.00 \times 10^{-11} \exp(-2500 \text{ K}/T) + 4.00 \times 10^{-13} \exp(775 \text{ K}/T) \quad (297 - 1376 \text{ K})$$

Keywords: Ketones; hydroxyl radicals; rate constants; shock tube; site-specific rates.

1. Introduction

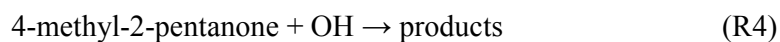
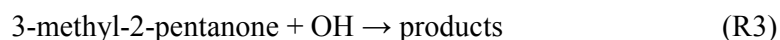
Biofuels will be a significant part of our future energy portfolio and are already experiencing widespread use in Europe and South America. Many innovative methods have recently been proposed to produce biofuels from biomass¹⁻³. One promising platform for cellulosic biofuel generation is to harness the metabolic processes of endophytic fungi that directly convert lignocellulosic material into a variety of volatile organic compounds including various types of saturated and unsaturated ketones⁴⁻⁸. Ketones are quite popular for their use as solvents. Ketones are also formed as intermediate compounds during the oxidation of large hydrocarbons or other oxygenated fuels, such as alcohols and ester. Significant amounts of ketones are emitted into the atmosphere and are thus considered ubiquitous air pollutants.

Hydroxyl (OH) is an important reactive radical in atmosphere and combustion systems, and it is widely accepted that OH radical oxidation of hydrocarbons and oxygenated species is the major oxidation route for these molecules under atmospheric and combustion conditions⁹⁻¹¹. A few studies have recently been carried out on the oxidation characteristics of ketones^{4-7, 12-21}. However, the reaction of ketones with OH and the overall oxidation chemistry of ketones are not well-known.

Previous investigations have mostly focused on smaller ketones. The smallest ketone, acetone, has drawn a lot of attention where its reaction with OH at a wide range of temperatures has been investigated thoroughly. Starting in 1991, Bott and Cohen²² were amongst the first to measure the rate constant of the reaction: acetone + OH \rightarrow products at high temperatures (\sim 1200 K). Subsequent to that, the rate constant of this reaction was measured by a number of other researchers^{18, 19, 21, 23-27}. Additionally, Zhao *et al.*²⁸ examined the reaction rate of acetone with atomic chlorine and Alzueta *et al.*¹⁴ inspected the oxidation of acetone with nitric oxide.

Other ketones have not been studied as thoroughly as acetone. The reaction rate of 2-butanone (methyl ethyl ketone or MEK) with OH has previously been investigated both experimentally^{23, 27} and theoretically¹⁸ at combustion temperatures. Also, the reaction of 2-butanone with atomic chlorine was studied to understand various abstraction channels²⁸. The same can be told about 3-pentanone where the rate constants for its reaction with chlorine²⁸ and OH^{18, 23, 27} have been investigated experimentally and numerically. Another isomer of pentanone, 2-pentanone, was studied at high temperature by Lam *et al.*²⁷ where they measured its reaction rate with OH. To our knowledge, the reaction of OH with ketones larger than C5 has not been studied previously at high temperatures.

The current work reports first direct measurement of the reaction of OH with large straight-chained and branched ketones at combustion temperatures. Measurements were carried out under pseudo-first-order conditions using a shock tube facility and narrow-linewidth UV laser absorption of OH. The rate constants for the reaction of 2-hexanone, 3-hexanone, 3-methyl-2-pentanone, and 4-methyl-2-pentanone with OH are measured at temperatures ranging 866 – 1375 K and pressures near 1.5 atm.



The measured high-temperature rate constant expressions are extended to lower temperatures by using low-temperature rate constant measurements from the literature. Additionally, previously measured high- and low- temperature rate constants for the reaction of OH with smaller ketones (acetone, 2-butanone, and 2-pentanone) are combined to formulate Arrhenius expressions applicable over wide temperatures.





Subsequent to that, the rate constants of above reactions (R1 – R7) are used to derive site-specific rate constants for H abstraction by OH from primary and secondary abstraction sites from ketones. This work reports, to our knowledge, the first experimentally determined site-specific H-abstraction rate constants for ketones. These new rate rules can be used to predict the rate constants of OH with a wider variety of molecules containing the carbonyl group.

2. Experimental Methods

Experiments were performed in the stainless steel, high-purity, low-pressure shock tube facility (LPST) at King Abdullah University of Science and Technology (KAUST). The method and experimental setup were detailed previously²⁹ and only a brief description is given here. The shock tube is made of a 9 m driver section and a 9 m driven section, with an inner diameter of 14.2 cm. The incident shock speed is measured using a series of five piezoelectric PCB pressure transducers over the last 1.3 m of the shock tube. Temperature and pressure behind reflected shock waves are determined from the measured incident shock speed and standard shock-jump relations. Uncertainties in the calculated temperature and pressure are approximately $\pm 0.7\%$ and $\pm 1\%$, respectively, mainly due to the uncertainty in the measured shock velocity ($\pm 0.2\%$). The facility is also equipped with a magnetically-stirred 24-litre mixing vessel and a well-furnished mixing manifold for the accurate preparation of mixtures. A double-dilution process was utilized when preparing mixtures to obtain more accurate concentrations in the mixing tank²⁷. The OH laser absorption diagnostic and a Kistler 603B piezoelectric pressure transducer are located at a test section 2 cm from the driven section endwall. Ultraviolet light for OH absorption is generated by the external frequency doubling of red light (614 nm) produced by a ring-dye cw laser which is pumped by a 10W green laser (532 nm). In the current experiments, UV light is tuned to the center

(306.6868 nm) of the well-characterized $R_1(5)$ absorption line in the OH A-X (0, 0) absorption band. A common-mode-rejection scheme is used here which gives a detection limit of about 0.2 ppm at 1400 K and 1 atm, assuming a minimum detectable absorbance of 0.1%. The OH mole fraction is calculated from Beer-Lambert law, $I/I_0 = \exp(-k_{OH}X_{OH}PL)$, where I and I_0 are the transmitted and incident laser intensities, k_{OH} is the OH absorption coefficient, X_{OH} is the OH mole fraction, P is the total pressure (atm), and L is the path length (14.2 cm). The estimated uncertainty in the measured OH mole fraction (X_{OH}) is approximately $\pm 3\%$, mainly due to the uncertainty in the reflected-shock temperature and OH absorption coefficient. Experimental data are recorded at a sampling rate of 2.5 MHz using a high-resolution (14 bit) data acquisition system.

Hydroxyl radicals were produced by rapid thermal decomposition of tert-butyl hydroperoxide (TBHP), where TBHP is known to be a clean OH precursor and has been validated in many studies^{25, 27, 29-35}. A 70% TBHP in water solution, 2-hexanone ($\geq 99.5\%$), 3-hexanone ($\geq 98\%$), 3-methyl-2-pentanone ($\geq 99\%$), and 4-methyl-2-pentanone ($\geq 99.5\%$) were obtained from Sigma Aldrich. Further purification is performed on all ketones by repeated freeze-pump-thaw cycles. Several reflected-shock experiments were conducted for each hexanone isomer. The concentrations of reactants (fuel, TBHP) were chosen carefully based on sensitivity analysis while maintaining pseudo-first-order conditions. Mixtures comprising approximately 200 ppm fuel, 10 – 20 ppm of TBHP (30-60 ppm of water) and balance argon were tested over the temperature range of 866 – 1376 K and pressures near 1.5 atm.

The CHEMKIN-PRO³⁶ commercial program was used to perform zero-dimensional simulations with constant internal energy and volume (constant UV) constraints. The fuels studied in this work do not have published chemical mechanisms and therefore sub-mechanisms for their reaction with OH are developed here. The sub-mechanism, comprising

of ketone + OH abstraction reactions and decomposition reactions of various abstraction products, of each fuel is added to the detailed kinetic mechanism of 3-pentanone developed by Serinyel *et al.*¹⁷. Additionally, a chemical model for the decomposition of TBHP and its subsequent radicals is added from Pang *et al.*³¹.

3. High-Temperature Measurements of Ketone + OH → Products

High-temperature rate constant measurements for the reaction of OH with four hexanone isomers are described in this section. A mixture of 200 ppm 2-hexanone ($C_4H_9COCH_3$), 17 ppm TBHP (45 ppm of water), and balance Ar was shock-heated to a range of post-shock temperatures (896 – 1370 K) and pressures near 1.5 atm to measure the reaction rate constant of 2-hexanone + OH → products. This reaction has five possible channels:



In order to develop a tentative sub-mechanism for 2-hexanone reaction with OH, we used the methodology proposed by Lam *et al.*²⁷ for their work on 2-pentanone. It is assumed that the fuel radical undergoes rapid decomposition to more stable intermediates (e.g. C_2H_4 and $CH_2CH_2COCH_3$) immediately after the H-abstraction process. Also, the rates of channels a, b, c, and d are assumed to be similar to the rates of H-abstraction by OH from methyl butanoate which are available in the kinetic mechanism of Dooley *et al.*³⁷. Channel e is assumed to be similar to channel c in the reaction of 2-butanone + OH²⁹. The decomposition reactions of the product C_3H_7CHCO (R1d) are assumed to be similar to those of C_2H_5CHCO , as given in¹⁷. The resulting branching ratios of channels 1a – 1e at a representative temperature of 1149 K are 0.21, 0.25, 0.25, 0.27, and 0.02. The sub-mechanism of 2-hexanone + OH is presented in

Table S1 in the Supplementary Material. Similar methodology is followed to develop sub-mechanisms for the reactions of 3-hexanone, 3-methyl-2-pentanone, and 4-methyl-2-pentanone with OH and these mechanisms are given in Tables S2 – S4 in the Supplementary Material. Also, a schematic of each molecule highlighting the nomination of H atoms (a, b, c, d, and e) is shown in the Supplementary Material.

Hydroxyl radical sensitivity analysis is performed for the 2-hexanone mixture at a representative temperature of 1149 K. The OH sensitivity is calculated as $S_{OH} = (\partial X_{OH} / \partial k_i) \times (k_i / X_{OH})$, where X_{OH} is the local OH mole fraction and k_i is the rate constant of the i th reaction. The sensitivity is plotted in Fig. 1 and shows that 2-hexanone + OH is the dominant reaction at the chosen conditions. However, minor interferences from secondary reactions occur and the rates for the important secondary reactions are updated based on the suggestions given in²⁹.

The experimentally measured OH profiles are fit using the cumulative mechanism comprising of the base mechanism¹⁷, sub-mechanism for 2-hexanone developed here, and TBHP reactions. The branching ratios of R1 are kept unchanged while fitting the experimental profiles. The overall rate constant ($k_1 = k_{1a} + k_{1b} + k_{1c} + k_{1d} + k_{1e}$) is insensitive to the branching ratios because of the pseudo-first-order conditions implemented here. This was verified by varying the branching ratios in the mechanism and this resulted in negligible effect on the measured overall rate constant. A raw trace of the measured OH time-history at 1149 K and 1.5 atm is presented in Fig. 2. The initial TBHP concentration for simulated profiles is taken from the experimental OH yield. The best-fit OH profile has a k_1 value of $2.55 \times 10^{-11} \text{ cm}^3 \text{ molecule}^{-1} \text{ s}^{-1}$ and the effect of 50% deviations from this value is also presented in Fig. 2. Measured values of rate constants for R1, along with the experimental conditions, are listed in Table 1.

Detailed uncertainty analysis was performed to estimate the errors in the measured rate constant for R1 at a representative condition of 1149 K and 1.5 atm. Various sources of errors considered here include the temperature ($\pm 0.7\%$), mixture composition ($\pm 5\%$), OH absorption coefficient ($\pm 3\%$), wavemeter reading ($\pm 0.002 \text{ cm}^{-1}$), errors in fitting the experimental profile ($\pm 5\%$), locating time zero ($\pm 0.5 \text{ }\mu\text{s}$), and rate constants of the secondary reactions. The contribution of each of these error sources on the determination of k_1 is analyzed separately. The overall uncertainty is calculated using the root-sum-squared method and is found to be $\pm 15\%$ for k_1 at 1149 K.

Arrhenius plot of the rate constant of 2-hexanone + OH \Rightarrow products is shown in Fig. 3. Rate constants calculated using the structure-reactivity approach (SAR)³⁸ are also shown in Fig. 3 with a multiplicative factor of 0.75. Lam *et al.*²⁷ showed that SAR calculations compared well with their experimental data of the reaction of OH with acetone, 2-butanone, 2-pentanone, and 3-pentanone when SAR predictions are multiplied by 0.75. Here, the same behavior is observed where the SAR method does a reasonable job of predicting the measured rate constants when multiplied by 0.75. The curve-fit of k_1 for the studied temperature range is also shown in Fig. 3 and it has the following Arrhenius expression:

$$k_1 = 1.24 \times 10^{-10} \exp(-1769 \text{ K}/T) \text{ cm}^3 \text{ molecule}^{-1} \text{ s}^{-1} \quad (896 - 1370 \text{ K}) \quad (1)$$

Similar procedure was used to measure the reaction rate constants for the reaction of OH with other three ketones. Fuel concentrations of 200 ppm were used for 3-hexanone, 3-methyl-2-pentanone, and 4-methyl-2-pentanone. Proportional amounts of TBHP that respect the pseudo-first-order (10 – 15 ppm) conditions were used to prepare ketone/TBHP/Ar mixtures. Experiments were carried out over a range of temperatures for each fuel and the OH time-histories were fit using the sub-mechanisms developed here. Uncertainty values for k_2 , k_3 , and k_4 are estimated to be $\pm 17\%$ at 1037 K, $\pm 17\%$ at 1049 K, and $\pm 16\%$ at 1063 K, respectively. Arrhenius plots for k_2 , k_3 , and k_4 are shown in Fig. 4, Fig. 5, and Fig. 6,

respectively. Predicted rate constants using the SAR estimation method are also shown. The SAR x 0.75 estimation method predicts the rate constants fairly well except for k_3 where it underestimates the measured values by about 10 – 15%. Measured rate constants for k_2 , k_3 , and k_4 are listed in Tables 2 – 4, and the corresponding Arrhenius expressions are:

$$k_2 = 1.73 \times 10^{-10} \exp(-2149 \text{ K}/T) \text{ cm}^3 \text{ molecule}^{-1} \text{ s}^{-1} \quad (876 - 1350 \text{ K}) \quad (2)$$

$$k_3 = 2.09 \times 10^{-10} \exp(-2629 \text{ K}/T) \text{ cm}^3 \text{ molecule}^{-1} \text{ s}^{-1} \quad (875 - 1344 \text{ K}) \quad (3)$$

$$k_4 = 2.42 \times 10^{-10} \exp(-2918 \text{ K}/T) \text{ cm}^3 \text{ molecule}^{-1} \text{ s}^{-1} \quad (866 - 1376 \text{ K}) \quad (4)$$

It is instructive to compare the measured rate constant data of the four isomers to analyze the effect of the position of the C=O bond as well as the methyl branching and its position. The rate constants for the reaction of OH with the four ketones are presented in Fig. 7; the SAR x 0.75 estimated rate constants are also shown. The position of the carbonyl group (C=O) does not affect the overall rate constant as can be observed from measured data and SAR calculations of 2- and 3-hexanone. Lam *et al.*²⁷ also showed that the position of C=O bond has negligible effect on the rate constants of 2- and 3-pentanone reactions with OH. On the other hand, the rate constants decrease when methyl branching occurs as can be seen from the experimental data and the SAR calculations of k_3 and k_4 compared with k_1 and k_2 . The position of the methyl branching has slight effect on the overall abstraction rate constant, where the rate constants decrease as the methyl branching moves further away from the carbonyl group (k_4 is slightly smaller than k_3). The SAR method does not reproduce this trend where the two lines (k_3 and k_4) overlap completely over the presented temperature range.

4. Site-Specific Rate Constants

To calculate the rate constants of various molecules with OH in the absence of experimental data, few estimation methods were developed over the years. In addition to the

structure-reactivity approach (SAR) of Atkinson and co-workers^{38, 39}, Cohen^{40, 41} used the group-additivity transition-state-theory (TST) method to reproduce the measurements of the rate constants of OH with a series of alkanes. The method of Cohen^{40, 41} was based on defining C-H bonds in alkanes according to the number of carbon atoms bonded to the next-nearest-neighbor (NNN) carbon. Recently, Sivaramakrishnan *et al.*^{42, 43} extended the work of Cohen^{40, 41} to determine three-parameter-fits for several site-specific H-abstraction rate constants. This was done with the aid of detailed high-level-ab-initio electronic structure theory computations of the molecular properties of reactants, products, and transition states. Their derived rates reproduce the experimental rate constants of OH with many alkanes including heavier molecules such as n-hexadecane. However, their site-specific rate constant expressions cannot be employed to calculate rate constants of the reactions of oxygenated molecules, such as ketones, with OH. In the current work, we have calculated site-specific rate constants over a very wide temperature range for molecules containing the carbonyl group. We employed the nomination of next-nearest-neighbor (N-N-N) which is based on an understanding that the primary, secondary, and tertiary C-H bonds are dependent on the number of C atoms bonded to the N-N-N carbon atom.

In order to derive the primary and secondary H-abstraction site-specific rate constants, the experimental data of the reaction of acetone, 2-butanone, and 2-pentanone with OH are also considered. Starting with acetone + OH reaction (k_5), data from Lam *et al.*²⁷ (872 – 1355 K), Vasudevan *et al.*²⁵ (982 – 1300 K), Yamada *et al.*²¹ (292 – 832 K), Tranter and Walker²³ (753 K), Wellington and Kurylo⁴⁴ (240 – 440 K), Wollenhaupt *et al.*⁴⁵ (202 – 395 K), and Gierczak *et al.*⁴⁶ (199 – 383 K) are evaluated here and these data are plotted in Fig. 8. Calculations from the SAR estimation method and the ab-initio theoretical study by Zhou *et al.*¹⁸ are also shown in Fig. 8, where the SAR method does a good job of predicting the experimental data for the entire temperature range. Theoretical calculations by Zhou *et al.*¹⁸

under-predict experimental data at intermediate and high temperatures and these calculations exhibit stronger curvature compared to the SAR method. The data presented in Fig. 8 are fit using two-Arrhenius expressions (T-A-E), $A \exp(-B/T) + C \exp(-D/T)$, as follows:

$$k_5 = 4.43 \times 10^{-13} \exp(-274 \text{ K}/T) + 5.50 \times 10^{-11} \exp(-2499 \text{ K}/T) \text{ cm}^3 \text{ molecule}^{-1} \text{ s}^{-1} \quad (285 - 1355 \text{ K}) \quad (5)$$

While the acetone + OH rate data could also have been fit using a single three-parameter Arrhenius expression, the rate data for 2-pentanone and 2-hexanone can only be adequately modeled with two Arrhenius expressions over the wider temperature range. Therefore, the acetone data were fit using two Arrhenius expressions to obtain consistent formulations. Acetone contains only one unique H-abstraction site. Having the expression for k_5 , the rate constant for primary H-abstraction by OH, from the α -CH₃ adjacent to the carbonyl group (C=O), can be calculated as:

$$P_{1,CO} = k_5/6 \quad (6)$$

The rate expression for this abstraction is:

$$P_{1,CO} = 7.38 \times 10^{-14} \exp(-274 \text{ K}/T) + 9.17 \times 10^{-12} \exp(-2499 \text{ K}/T) \text{ cm}^3 \text{ molecule}^{-1} \text{ s}^{-1} \quad (285 - 1355 \text{ K}) \quad (7)$$

For the reaction of 2-butanone with OH (k_6), the data from Badra *et al.*²⁹ (979 – 1464 K), Lam *et al.*²⁷ (879 – 1364 K), Tranter and Walker²³ (753 K), Carr *et al.*⁴⁷ (213 – 598 K), Wallington and Kurylo⁴⁴ (240 – 440 K), Jiménez *et al.*⁴⁸ (228 – 388 K), and Le Calvé *et al.*⁴⁹ (243 – 372 K) are plotted in Fig. 9 along with the SAR estimation method, the ab-initio calculations by Zhou *et al.*¹⁸, and the T-A-E (two-Arrhenius expressions) fit derived here. The SAR method fails to reproduce the experimental data at intermediate and low temperatures.

Also, the ab-initio calculations by Zhou *et al.*¹⁸ fall short in the intermediate and low temperature range and again exhibit significantly stronger curvature in the rate constant profile. The derived T-A-E for k_6 is:

$$k_6 = 9.93 \times 10^{-11} \exp(-2392 \text{ K}/T) + 1.25 \times 10^{-12} \exp(-51 \text{ K}/T) \text{ cm}^3 \text{ molecule}^{-1} \text{ s}^{-1} \quad (222 - 1464 \text{ K}) \quad (8)$$

According to the N-N-N estimation method, k_6 can be written in terms of site-specific rate constants as follows:

$$k_6 = 3P_{1,CO} + 2S_{10,CO} + 3P_1 \quad (9)$$

where $S_{10,CO}$ is the rate constant for secondary H-abstraction by OH from the methylene group ($-\text{CH}_2-$) adjacent to the carbonyl group, P_1 is the rate constant for primary H-abstraction by OH from the methyl group ($-\text{CH}_3$) at site 4 (adjacent to CH_2 group), and $P_{1,CO}$ is the same as defined for acetone. The P_1 rate constant is assumed to be the same as in alkanes since it is not neighboring the carbonyl group and therefore the expression derived by Sivaramakrishnan and Michael⁴² for P_1 is implemented here. Solving Eq. (9), $S_{10,CO}$ has the following T-A-E (two-Arrhenius expression):

$$S_{10,CO} = 1.20 \times 10^{-11} \exp(-2046 \text{ K}/T) + 2.20 \times 10^{-13} \exp(160 \text{ K}/T) \text{ cm}^3 \text{ molecule}^{-1} \text{ s}^{-1} \quad (222 - 1464 \text{ K}) \quad (10)$$

The $S_{10,CO}$ rate constant expression has negative temperature dependence at low temperatures which is in agreement with the fact that k_6 is almost constant at low temperatures whereas $P_{1,CO}$ (and k_5) shows strong positive temperature dependence.

For the reaction of 2-pentanone with OH (k_7), the data from Lam *et al.*²⁷ (902 – 1302 K), Jiménez *et al.*⁴⁸ (248 – 388 K), Atkinson *et al.*⁵⁰ (299 K), Atkinson *et al.*⁵¹ (298 K), and Wallington and Kurylo⁴⁴ (298 K) are plotted in Fig. 10 along with the SAR calculations. The

SAR method fails to reproduce intermediate and low temperature data and does not exhibit the negative temperature dependence at low temperatures. The T-A-E fit derived here captures the high and low temperature data very well, and is given as:

$$k_7 = 9.50 \times 10^{-11} \exp(-1800 \text{ K}/T) + 2.70 \times 10^{-13} \exp(750 \text{ K}/T) \text{ cm}^3 \text{ molecule}^{-1} \text{ s}^{-1} \quad (248 - 1302 \text{ K}) \quad (11)$$

Using the N-N-N nomination method, the rate constant of 2-pentanone with OH can be written as:

$$k_7 = 3P_{1,CO} + 2S_{11,CO} + 2S_{10} + 3P_1 \quad (12)$$

where $S_{11,CO}$ is the rate constant for secondary H-abstraction by OH from the methylene group ($-\text{CH}_2-$) adjacent to the carbonyl group and S_{10} is the rate constant for secondary H-abstraction by OH from the methylene group ($-\text{CH}_2-$) at site 4. Here, P_1 and $P_{1,CO}$ rate constants are same as defined earlier. The S_{10} rate constant is assumed to be the same as found in alkanes since it is not neighboring the carbonyl group. Therefore, the expression derived by Sivaramakrishnan and Michael⁴² for S_{10} is used here. Solving Eq. (12), rate constant expression for $S_{11,CO}$ can be derived:

$$S_{11,CO} = 4.50 \times 10^{-11} \exp(-3000 \text{ K}/T) + 8.50 \times 10^{-15} \exp(1440 \text{ K}/T) \text{ cm}^3 \text{ molecule}^{-1} \text{ s}^{-1} \quad (248 - 1302 \text{ K}) \quad (13)$$

The current experimental data of 2-hexanone + OH (k_1) are extended to low temperatures by using the data from Jiménez *et al.*⁴⁸ (263 – 405 K), Atkinson and Aschmann³⁶ (296 K), Atkinson *et al.*⁵⁰ (299 K), and Wallington and Kurylo⁴⁴ (296 K). These data are presented in Fig. 11 along with the SAR calculations and the T-A-E derived here, which has the following expression:

$$k_1 = 1.28 \times 10^{-10} \exp(-1852 \text{ K}/T) + 4.86 \times 10^{-13} \exp(764 \text{ K}/T) \text{ cm}^3 \text{ molecule}^{-1} \text{ s}^{-1} \quad (263 - 1370 \text{ K}) \quad (14)$$

Similar to the 2-pentanone case, the SAR method cannot reproduce the rate constant data of 2-hexanone + OH at low and intermediate temperatures, whereas the T-A-E developed in this work does a very good job of capturing the data at all temperatures. The rate constant of 2-hexanone + OH can be expressed in terms of site-specific rate constants as follows:

$$k_1 = 3P_{1,CO} + 2S_{11',CO} + 2S_{11} + 2S_{10} + 3P_1 \quad (15)$$

where $S_{11\Box,CO}$ is rate constant for the secondary H-abstraction by OH from the methylene group ($-\text{CH}_2-$) adjacent to the carbonyl group. The prime symbol indicates that this methylene group is neighboring an S_{11} and not S_{10} . Here, S_{11} is the rate constant for secondary H-abstraction by OH from the methyl group ($-\text{CH}_3$) at site 4. The S_{11} rate constant is assumed to be the same as found in alkanes since it is not neighboring the carbonyl group and therefore the expression derived by Sivaramakrishnan and Michael⁴² is used here. $S_{11\Box,CO}$ has the following T-A-E after solving Eq. (15):

$$S_{11',CO} = 3.80 \times 10^{-11} \exp(-2500 \text{ K}/T) + 8.50 \times 10^{-15} \exp(1550 \text{ K}/T) \text{ cm}^3 \text{ molecule}^{-1} \text{ s}^{-1} \quad (263 - 1370 \text{ K}) \quad (16)$$

The current high-temperature experimental data of OH + 4-methyl-2-pentanone (k_4) along with the data from Le Calvé *et al.*⁴⁹ (253 – 372 K), Winer *et al.*⁵² (305 K), Atkinson *et al.*⁵⁰ (299 K), and O'Rji and Stone⁵³ (297 K) are presented in Fig. 12. The SAR estimation method and the T-A-E fitting, which has the following expression, are also shown in Fig. 12.

$$k_4 = 2.00 \times 10^{-10} \exp(-2800 \text{ K}/T) + 9.30 \times 10^{-13} \exp(775 \text{ K}/T) \text{ cm}^3 \text{ molecule}^{-1} \text{ s}^{-1} \quad (297 - 1376 \text{ K}) \quad (17)$$

According to the N-N-N estimation method, k_4 can be written in terms of site-specific rate constants as follows:

$$k_4 = 3P_{1,CO} + 2S_{21,CO} + T_{100} + 6P_2 \quad (18)$$

where $S_{21,CO}$ is the rate constant for secondary H-abstraction by OH from the methylene group ($-\text{CH}_2-$) adjacent to the carbonyl group and T_{100} is the rate constant for tertiary H-abstraction by OH from the methylidyne group ($-\text{CH}-$) at site 4 (adjacent to CH_2 group). The T_{100} rate constant is assumed to be the same as in alkanes since it is not neighboring the carbonyl group and, therefore, the expression derived by Badra *et al.*⁵⁴ for T_{100} is implemented here. Solving Eq. (18), $S_{21,CO}$ has the following expression:

$$S_{21,CO} = 5.00 \times 10^{-11} \exp(-2500 \text{ K}/T) + 4.00 \times 10^{-13} \exp(775 \text{ K}/T) \text{ cm}^3 \text{ molecule}^{-1} \text{ s}^{-1} (297 - 1376 \text{ K}) \quad (19)$$

The rate constant of 3-methyl-2-pentanone + OH \rightarrow products (k_3) can be written in terms of site-specific rate constants using the N-N-N method as follows:

$$k_3 = 3P_{1,CO} + T_{110,CO} + 3P_{2,CO} + 2S_{20} + 3P_1 \quad (20)$$

where $T_{110,CO}$ and $P_{2,CO}$ are the rates for tertiary and primary H-abstraction by OH from the methylidyne ($-\text{CH}-$) and methyl ($-\text{CH}_3$) groups adjacent to the carbonyl group, respectively. However, this expression (Eq. (20)) has two unknowns ($T_{110,CO}$ and $P_{2,CO}$) and further experiments will be needed to determine these site-specific rate constants. For example, the rate constant of 3,3-dimethyl-2-butanone with OH enables the determination of $P_{3,CO}$ and then $P_{2,CO}$ can be estimated as the average of $P_{1,CO}$ and $P_{3,CO}$. Subsequent to that, $T_{110,CO}$ can be calculated from Eq. (20).

The determined rate constants for site-specific H-abstraction from carbon atoms adjacent to the carbonyl group are listed in Table 5. The parameters for the other site-specific

rate constants, which are same as in alkanes, can be found in^{42, 54}. The rate constant of OH with straight-chained ketones of any carbon number can now be estimated using the N-N-N method since all relevant site-specific rate constants have been derived. Also, the rate constants of any singly-methylated branched ketone can be estimated using the determined site-specific rate constants. The calculated site-specific rate constants are presented in Fig. 13 along with the relevant site-specific rates calculated by Zhou *et al.*¹⁸. As can be seen from Fig. 13, the calculated primary and secondary site-specific rate constants by Zhou *et al.*¹⁸ do not agree with our experimental determinations. This discrepancy was observed earlier in the form of total rate constants of acetone (Fig. 8) and 2-butanone (Fig. 9). Additionally, Figure 13 clearly shows that secondary H-abstraction rate constants exhibit the negative temperature dependence at low temperatures.

The validity of the calculated site-specific rate constants is evaluated here by comparing calculated rate constants with experimental data for the reaction of OH with 3-pentanone, 3-hexanone, and 2-heptanone. Using the N-N-N nomination method, these rate constants can be written as:

$$k_{3\text{-pentanone}+\text{OH}} = 6P_1 + 4S_{10,\text{CO}} \quad (21)$$

$$k_{3\text{-hexanone}+\text{OH}} = 6P_1 + 2S_{10,\text{CO}} + 2S_{11,\text{CO}} + 2S_{10} \quad (22)$$

$$k_{2\text{-heptanone}+\text{OH}} = 3P_{10,\text{CO}} + 2S_{11',\text{CO}} + 2S_{11'} + 2S_{11} + 2S_{10} + 3P_1 \quad (23)$$

Regarding the reaction of 3-pentanone with OH, the data from Lam *et al.*²⁷ (878 – 1353 K), Wallington and Kurylo⁴⁴ (240 – 440 K), Atkinson *et al.*⁵⁰ (299 K), and Atkinson and Aschmann³⁶ (296 K) are plotted in Fig. 14 along with SAR and our N-N-N calculations. Both estimation methods reproduce the high temperature data very well. However, the SAR method fails to reproduce the negative temperature dependence at low temperatures. The N-N-N method agrees quite well with the ambient temperature data from Atkinson and co-

workers^{36, 50} but underestimates the data from Wallington and Kurylo⁴⁴. This discrepancy can be attributed to the relatively large uncertainty in the experimental measurements of Wallington and Kurylo⁴⁴ where their measured data for acetone, 2-butanone, and 2-pentanone were also higher than other measurements, as can be seen from Fig. 8, Fig. 9, and Fig. 10.

For the reaction of 3-hexanone with OH (k_2), the current high-temperature experimental data are presented in Fig. 15 along with the only available low temperature measurement of Atkinson *et al.*⁵⁰ (299 K). The SAR and N-N-N calculations from current work are also plotted in Fig. 15. The N-N-N method agrees very well with the experimental data at high temperatures, however, it underestimates the single-temperature measurement of Atkinson *et al.*⁵⁰. The data from Atkinson *et al.*⁵⁰ are generally higher than other literature data at corresponding temperature, as was the case for 2-pentanone (Fig. 10), 2-hexanone (Fig. 11), and 2-heptanone (Fig. 16). Thus it is not surprising that the N-N-N method underestimates the Atkinson *et al.*⁵⁰ rate constant measurement for 3-hexanone + OH at 299 K. It can be argued that more data are needed for the reaction of OH with 3-pentanone and 3-hexanone at low temperatures for further verification of the calculated site-specific rate constants.

High-temperature rate constant data are not available for the reaction of 2-heptanone with OH. Low-temperature data from Jiménez *et al.*⁴⁸ (260 – 405 K), Atkinson *et al.*⁵⁰ (299 K), and Wallington and Kurylo⁴⁴ (296 K) are plotted in Fig. 16 along with the SAR and N-N-N calculations. The N-N-N method agrees very well with the low temperature data of Jiménez *et al.*⁴⁸ and Wallington and Kurylo⁴⁴. Additionally, the negative temperature dependence is successfully reproduced by the N-N-N calculation. As expected, SAR method is unable to capture the low temperature rate constant data.

5. Conclusions

We have conducted ketone + OH reaction rate constant measurements behind reflected shock waves. Measurements were carried out for large normal (2-hexanone and 3-hexanone) and branched (3-methyl-2-pentanone and 4-methyl-2-pentanone) ketones over 866 – 1375 K. This work presents, to our knowledge, the first high-temperature rate constant measurements for the reaction of OH with the four hexanone isomers. The current high temperature data, and previous measurements of the reaction of OH with acetone, 2-butanone, and 2-pentanone, are extended to low temperatures and fit with two-Arrhenius expressions. Finally, new site-specific rate constants are derived for H-abstraction by OH from ketones. These site-specific rate constants will be extremely helpful in calculating the rate of the OH + ketone reaction for other ketones and in evaluating the branching ratios of these abstraction reactions. We believe the results of this paper will stir up new ab-initio calculations of the ketone-specific rate constants.

6. Acknowledgements

We would like to acknowledge the funding support from Saudi Aramco under the FUELCOM program. We are also thankful for the financial support provided by the Clean Combustion Research Center (CCRC) and King Abdullah University of Science and Technology (KAUST).

7. Supplementary Materials:

Tables of sub-mechanisms developed for the four hexanone isomers are provided.

8. References

1. M. A. Rude and A. Schirmer, *Curr. Opin. Microbiol.*, 2009, **12**, 274-281.
2. K. Kohse-Höinghaus, P. Oßwald, T. A. Cool, T. Kasper, N. Hansen, F. Qi, C. K. Westbrook and P. R. Westmoreland, *Angew. Chem. Int. Ed.*, 2010, **49**, 3572-3597.
3. T. Liu and C. Khosla, *Annu. Rev. Genet.*, 2010, **44**, 53-69.
4. M. Stadler and B. Schulz, *Trends in Plant Science*, 2009, **14**, 353-355.
5. M. A. Griffin, D. J. Spakowicz, T. A. Gianoulis and S. A. Strobel, *Microbiology* 2010, **156**, 3814–3829.
6. S. K. Singh, G. A. Strobel, B. Knighton, B. Geary, J. Sears and D. Ezra, *Microb Ecol*, 2011, **61**, 729-739.
7. G. A. Strobel, B. Knighton, K. Kluck, Y. Ren, T. Livinghouse, M. A. Griffin, D. J. Spakowicz and J. Sears, *Microbiology*, 2008, **154**, 3319–3328.
8. M. T. Mends, E. Yu, G. A. Strobel, S. Riyaz-Ul-Hassan, E. Booth, B. Geary, J. Sears, C. A. Taatjes and M. S. Hadi, *J. Pet Environ Biotechnol*, 2012, **3:117**.
9. S. S. Vasu, D. F. Davidson and R. K. Hanson, *Combust. Flame*, 2009, **156**, 736.
10. J. Zádor, A. W. Jasper and J. A. Miller, *Phys. Chem. Chem. Phys.*, 2009, **11**, 11040.
11. J. F. Bott and N. Cohen, *Int. J. Chem. Kinet.*, 1991, **23**, 1075.
12. S. S. Vasu, O. Welz, D. L. Osborn and C. A. Taatjes, *7th International Conference on Gas Kinetics*, 2011.
13. S. S. Vasu, O. Welz, D. L. Osborn and C. A. Taatjes, *7th U.S. National Combustion Meeting*, 2011.
14. M. U. Alzueta, Z. Serinyel, J. M. Simmie and H. J. Curran, *Energy & Fuels*, 2010, **24**, 1511-1520.
15. G. Black, S. Pichon, H. Curran, J. Simmie, R. Donohue and N. Djebaili-Chaumeix, in *Third European Combustion Meeting ECM*, 2007.

16. Z. Serinyel, G. Black, H. J. Curran and J. M. Simmie, *Combust. Sci. Technol.*, 2010, **182**, 574-587.
17. Z. Serinyel, N. Chaumeix, G. Black, J. M. Simmie and H. J. Curran, *J. Phys. Chem. A*, 2010, **114**, 12176-12186.
18. C. Zhou, J. Simmie and H. Curran, *Phys. Chem. Chem. Phys.*, 2011, **13**, 11175-11192.
19. S. Canneaux, N. Slokolowski-Gomez, E. Henon, F. Bohr and S. Dobe, *Phys. Chem. Chem. Phys.*, 2004, **6**, 5172-5177.
20. B. Chuong and P. S. Stevens, *J. Phys. Chem. A*, 2003, **107**, 2185-2191.
21. T. Yamada, P. H. Taylor, A. Goumri and P. Marshall, *J. Chem. Phys.*, 2003, **119**, 10600-10606.
22. J. F. Bott and N. Cohen, *Int. J. Chem. Kinet.*, 1991, **23**, 1017-1033.
23. R. S. Tranter and R. W. Walker, *Phys. Chem. Chem. Phys.*, 2001, **3**, 1262-1270.
24. J. D. Raff, P. S. Stevens and R. A. Hites, *J. Phys. Chem. A*, 2005, **109**, 4728-4735.
25. V. Vasudevan, D. F. Davidson and R. K. Hanson, *J. Phys. Chem. A*, 2005, **109**, 3352-3359.
26. N. K. Srinivasan, M. C. Su and J. V. Michael, *J. Phys. Chem. A*, 2007, **111**, 3951-3958.
27. K. Lam, D. Davidson and R. Hanson, *J. Phys. Chem. A*, 2012, **116**, 5549-5559.
28. Z. Zhao, D. T. Huskey, J. M. Nicovich and P. H. Wine, *Int. J. Chem. Kinet.*, 2008, **40**, 259-267.
29. J. Badra, A. Elwardany, F. Khaled, S. S. Vasu and A. Farooq, *Combust. Flame*, 2014, **161**, 725-734.
30. Z. Hong, S. S. Vasu, D. F. Davidson and R. K. Hanson, *J. Phys. Chem. A*, 2010, **114**, 5520-5525.

31. G. A. Pang, R. K. Hanson, D. M. Golden and C. T. Bowman, *Z. Phys. Chem.*, 2011, **225**, 1157-1178.
32. G. A. Pang, R. K. Hanson, D. M. Golden and C. T. Bowman, *J. Phy. Chem. A*, 2012, **116**, 2475-2483.
33. G. A. Pang, R. K. Hanson, D. M. Golden and C. T. Bowman, *J. Phy. Chem. A*, 2012, **116**, 4720-4725.
34. S. S. Vasu, D. F. Davidson, R. K. Hanson and D. M. Golden, *Chem. Phys. Lett.*, 2010, **497**, 26-29.
35. S. S. Vasu, Z. Hong, D. F. Davidson, R. K. Hanson and D. M. Golden, *The Journal of Physical Chemistry A*, 2010, **114**, 11529-11537.
36. R. Atkinson and S. M. Aschmann, *J. Phys. Chem.*, 1988, **92**, 4008-4008.
37. S. Dooley, H. J. Curran and J. M. Simmie, *Combust. Flame*, 2008, **153**, 2-32.
38. E. S. C. Kwok and R. Atkinson, *Atmos. Environ.*, 1995, **29**, 1685-1695.
39. R. Atkinson, *Chem. Rev.*, 1986, **86**, 69-201.
40. N. Cohen, *Int. J. Chem. Kinet.*, 1982, **14**, 1339-1362.
41. N. Cohen, *Int. J. Chem. Kinet.*, 1991, **23**, 397-417.
42. R. Sivaramakrishnan and J. V. Michael, *J. Phy. Chem. A*, 2009, **113**, 5047-5060.
43. R. Sivaramakrishnan, N. K. Srinivasan, M. C. Su and J. V. Michael, *Proc. Combust. Inst.*, 2009, **32**, 107-114.
44. T. J. Wallington and M. J. Kurylo, *J. Phys. Chem.*, 1987, **91**, 5050-5054.
45. M. Wollenhaupt, S. A. Carl, A. Horowitz and J. N. Crowley, *J. Phy. Chem. A*, 2000, **104**, 2695-2705.
46. T. Gierczak, M. K. Gilles, S. Bauerle and A. R. Ravishankara, *J. Phy. Chem. A*, 2003, **107**, 5014-5020.

47. S. A. Carr, M. T. Baeza-Romero, M. A. Blitz, B. J. S. Price and P. W. Seakins, *Int. J. Chem. Kinet.*, 2008, **40**, 504-514.
48. E. Jiménez, B. Ballesteros, E. Martínez and J. Albaladejo, *Environ. Sci. Technol.*, 2005, **39**, 814-820.
49. S. Le Calvé, D. Hitier, G. Le Bras and A. Mellouki, *J. Phy. Chem. A*, 1998, **102**, 4579-4584.
50. R. Atkinson, S. M. Aschmann, W. P. L. Carter and J. N. Pitts, *Int. J. Chem. Kinet.*, 1982, **14**, 839-847.
51. R. Atkinson, E. C. Tuazon and S. M. Aschmann, *Environ. Sci. Technol.*, 2000, **34**, 623-631.
52. A. M. Winer, A. C. Lloyd, K. R. Darnall and J. N. Pitts, *J. Phys. Chem.*, 1976, **80**, 1635-1639.
53. L. N. O'Rji and D. A. Stone, *Int. J. Chem. Kinet.*, 1992, **24**, 703-710.
54. J. Badra, A. Elwardany and A. Farooq, *Proc. Combust. Inst.*, 2014, **Accepted**.

Table 1. High-temperature rate constant data for 2-hexanone + OH \rightarrow Products.

T_5 (K)	P_5 (atm)	k_1 ($\text{cm}^3 \text{ molecule}^{-1} \text{ s}^{-1}$)
896	1.69	1.78×10^{-11}
959	1.64	2.01×10^{-11}
1028	1.54	2.20×10^{-11}
1149	1.50	2.55×10^{-11}
1236	1.41	2.81×10^{-11}
1297	1.37	3.09×10^{-11}
1370	1.34	3.71×10^{-11}

Table 2. High-temperature rate constant data for 3-hexanone + OH \rightarrow Products.

T_5 (K)	P_5 (atm)	k_2 ($\text{cm}^3 \text{ molecule}^{-1} \text{ s}^{-1}$)
876	1.68	1.60×10^{-11}
944	1.59	1.79×10^{-11}
1037	1.57	2.04×10^{-11}
1139	1.47	2.53×10^{-11}
1214	1.37	2.92×10^{-11}
1278	1.34	3.19×10^{-11}
1350	1.30	3.70×10^{-11}

Table 3. High-temperature rate constant data for 3-methyl-2-pentanone + OH \rightarrow Products.

T_5 (K)	P_5 (atm)	k_3 ($\text{cm}^3 \text{ molecule}^{-1} \text{ s}^{-1}$)
875	1.69	1.09×10^{-11}
906	1.64	1.24×10^{-11}
942	1.58	1.32×10^{-11}
994	1.55	1.43×10^{-11}
1049	1.49	1.59×10^{-11}
1135	1.46	2.01×10^{-11}
1185	1.45	2.14×10^{-11}
1231	1.40	2.26×10^{-11}
1271	1.33	2.50×10^{-11}
1344	1.32	2.90×10^{-11}

Table 4. High-temperature rate constant data for 4-methyl-2-pentanone + OH \rightarrow Products.

T_5 (K)	P_5 (atm)	k_4 ($\text{cm}^3 \text{ molecule}^{-1} \text{ s}^{-1}$)
866	1.66	8.86×10^{-12}
918	1.68	1.14×10^{-11}
971	1.67	1.24×10^{-11}
1005	1.58	1.31×10^{-11}
1063	1.53	1.47×10^{-11}
1144	1.49	1.69×10^{-11}
1185	1.45	2.02×10^{-11}
1245	1.43	2.11×10^{-11}
1293	1.37	2.49×10^{-11}
1376	1.34	3.10×10^{-11}

Table 5. Rate constants for H-abstraction by OH from ketones according to the expression

$$A \exp(-B/T) + C \exp(-D/T) \text{ cm}^3 \text{ molecule}^{-1} \text{ s}^{-1}.$$

Site-specific rate constant	A	B	C	D
P _{1,CO}	7.38 x 10 ⁻¹⁴	274	9.17 x 10 ⁻¹²	2499
S _{10,CO}	1.20 x 10 ⁻¹¹	2046	2.20 x 10 ⁻¹³	-160
S _{11,CO}	4.50 x 10 ⁻¹¹	3000	8.50 x 10 ⁻¹⁵	-1440
S _{11□,CO}	3.80 x 10 ⁻¹¹	2500	8.50 x 10 ⁻¹⁵	-1550
S _{21,CO}	5.00 x 10 ⁻¹¹	2500	4.00 x 10 ⁻¹³	-775

Figure Captions:

Fig. 1. OH sensitivity for the rate constant measurement of 2-hexanone + OH at 1149 K and 1.5 atm. Initial mixture: 200 ppm 2-hexanone, 17 ppm TBHP (50 ppm water), balance Ar.

Fig. 2. 2-hexanone + OH reaction rate measurement at 1149 K and 1.5 atm. The best-fit simulated profile and perturbations of $\pm 50\%$ are also presented.

Fig. 3. Arrhenius plot of 2-hexanone + OH \rightarrow products.

Fig. 4. Arrhenius plot of 3-hexanone + OH \rightarrow products.

Fig. 5. Arrhenius plot of 3-methyl-2-pentanone + OH \rightarrow products.

Fig. 6. Arrhenius plot of 4-methyl-2-pentanone + OH \rightarrow products.

Fig. 7. Arrhenius plot of k_1 , k_2 , k_3 , and k_4 . Scatter points are experimental data measured here and lines represent SAR calculations.

Fig. 8. Arrhenius plot of acetone + OH \rightarrow Products for the temperature range of 285 – 1355 K.

Fig. 9. Arrhenius plot of 2-butanone + OH \rightarrow Products for the temperature range of 222 – 1464 K.

Fig. 10. Arrhenius plot of 2-pentanone + OH \rightarrow Products for the temperature range of 248 – 1302 K.

Fig. 11. Arrhenius plot of 2-hexanone + OH \rightarrow Products for the temperature range of 263 – 1370 K.

Fig. 12. Arrhenius plot of 4-methyl-2-pentanone + OH \rightarrow Products for the temperature range of 297 – 1376 K.

Fig. 13. Arrhenius plot of the various site-specific rate constants for the temperature range of 250 – 1450 K.

Fig. 14. Arrhenius plot of 3-pentanone + OH \rightarrow Products for the temperature range of 240 – 1353 K.

Fig. 15. Arrhenius plot of 3-hexanone + OH \rightarrow Products for the temperature range of 299 – 1350 K.

Fig. 16. Arrhenius plot of 2-heptanone + OH \rightarrow Products for the temperature range of 260 – 1450 K.

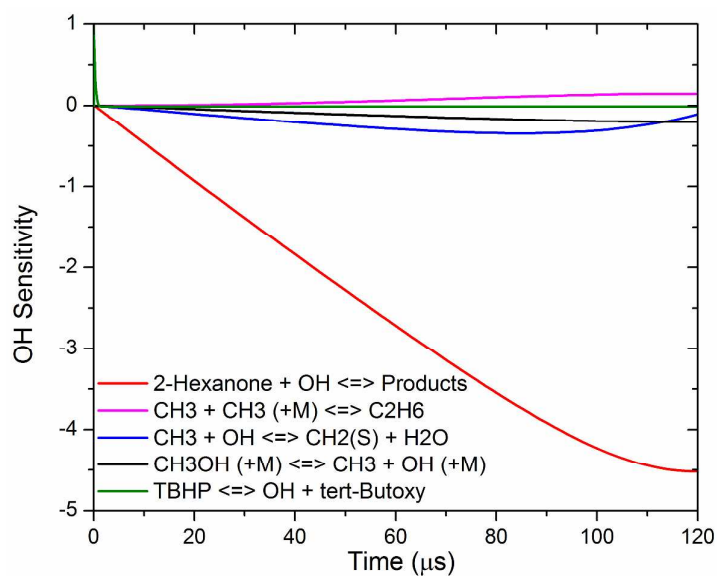


Fig. 1. OH sensitivity for the rate constant measurement of 2-hexanone + OH at 1149 K and 1.5 atm. Initial mixture: 200 ppm 2-hexanone, 17 ppm TBHP (50 ppm water), balance Ar.

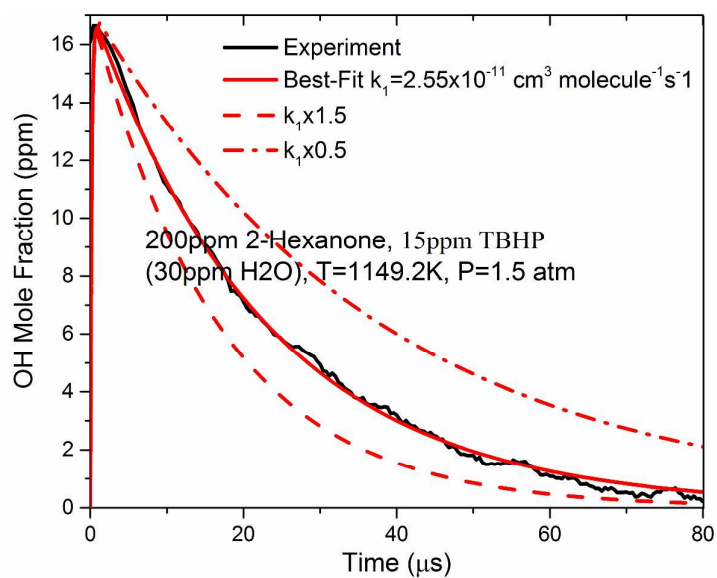


Fig. 2. Rate constant measurements for 2-hexanone + OH reaction at 1149 K and 1.5 atm. The best-fit simulated profile and perturbations of $\pm 50\%$ are also presented.

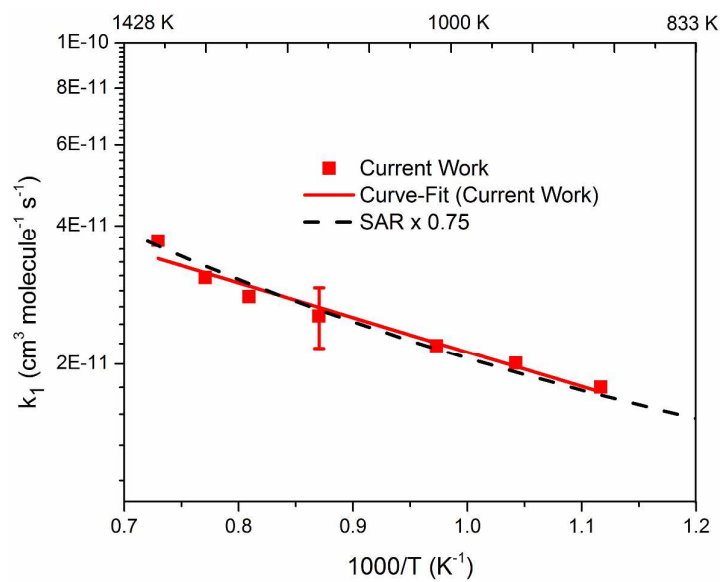


Fig. 3. Arrhenius plot of 2-hexanone + OH \rightarrow products.

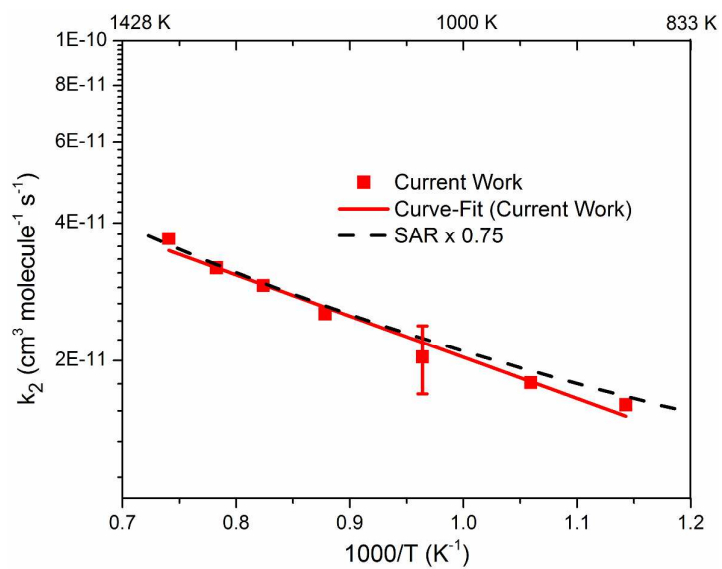


Fig. 4. Arrhenius plot of 3-hexanone + OH \rightarrow products.

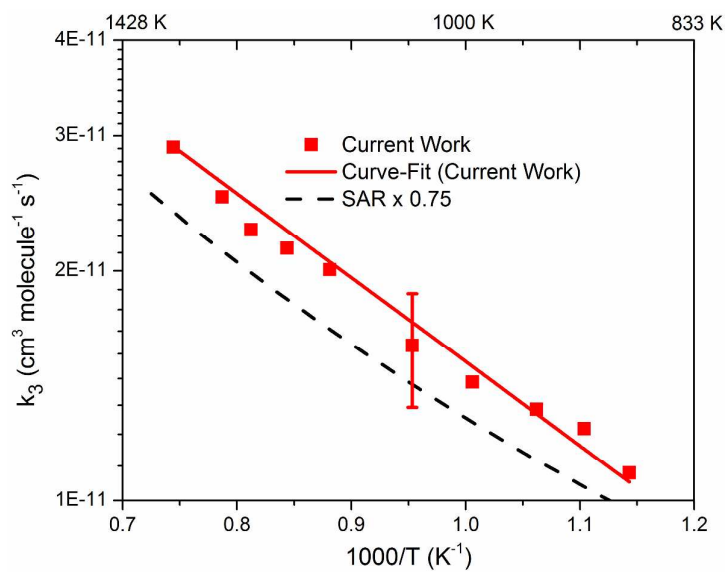


Fig. 5. Arrhenius plot of 3-methyl-2-pentanone + OH \rightarrow products.

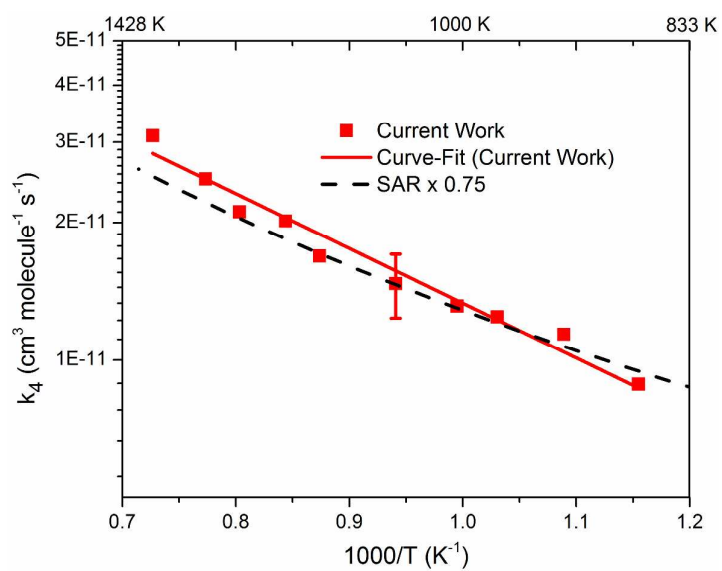


Fig. 6. Arrhenius plot of 4-methyl-2-pentanone + OH \rightarrow products.

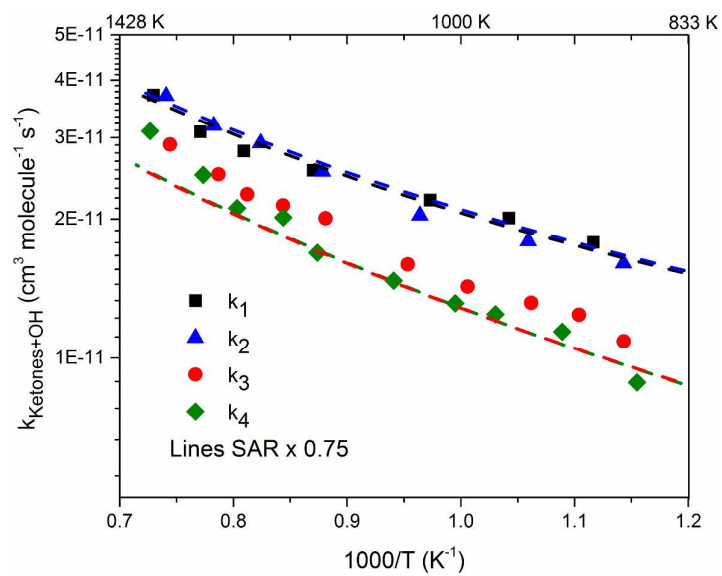


Fig. 7. Arrhenius plot of k_1 , k_2 , k_3 , and k_4 . Scatter points are experimental data measured here and lines represent SAR calculations.

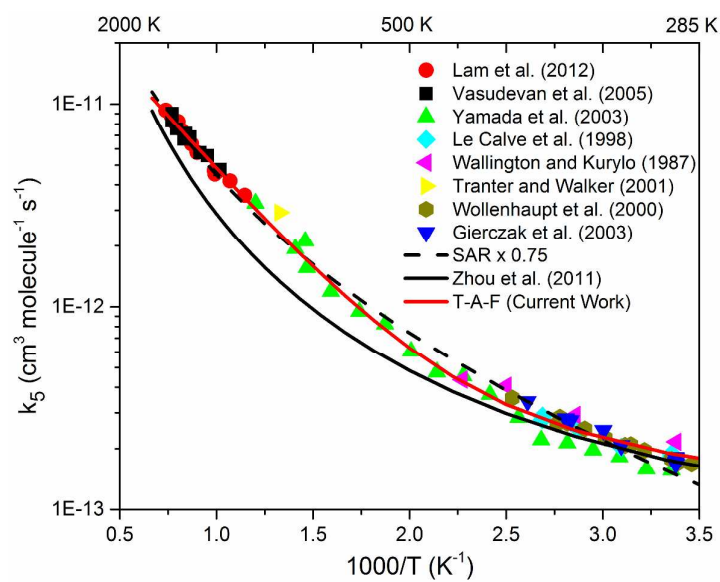


Fig. 8. Arrhenius plot of acetone + OH \rightarrow Products for the temperature range of 285 – 1355

K.

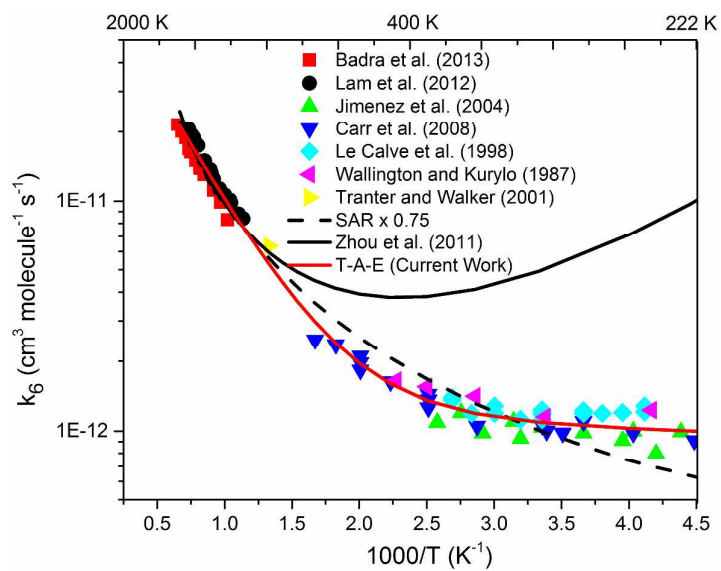


Fig. 9. Arrhenius plot of 2-butanone + OH \rightarrow Products for the temperature range of 222 – 1464 K.

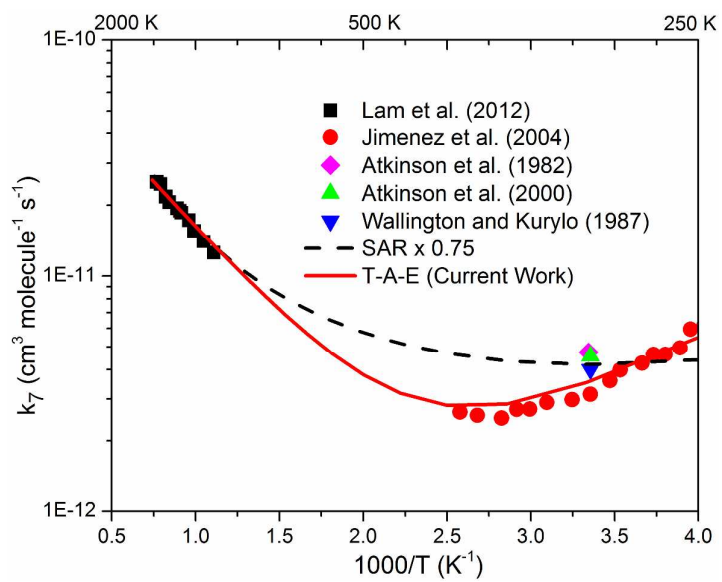


Fig. 10. Arrhenius plot of 2-pentanone + OH → Products for the temperature range of 248 – 1302 K.

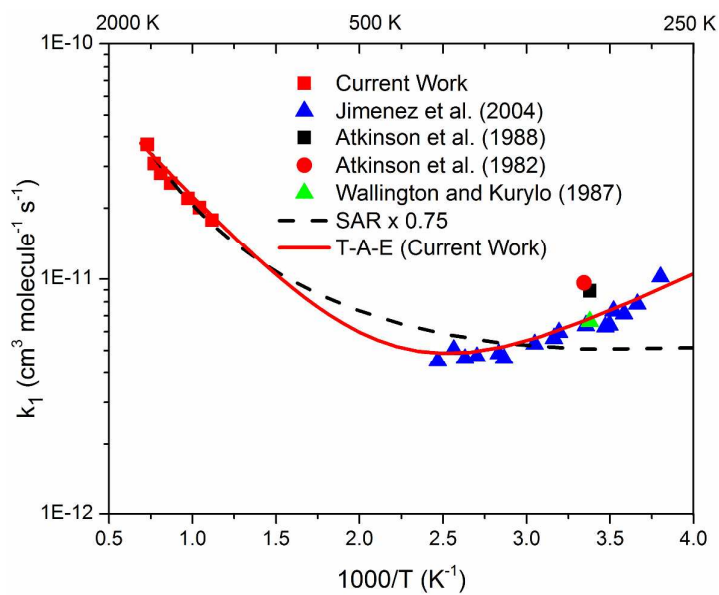


Fig. 11. Arrhenius plot of 2-hexanone + OH \rightarrow Products for the temperature range of 263 – 1370 K.

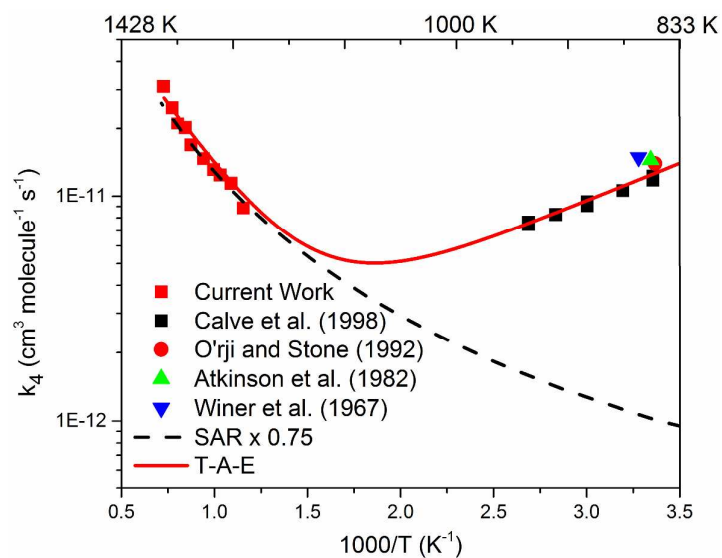


Fig. 12. Arrhenius plot of 4-methyl-2-pentanone + OH \rightarrow Products for the temperature range of 297 – 1376 K.

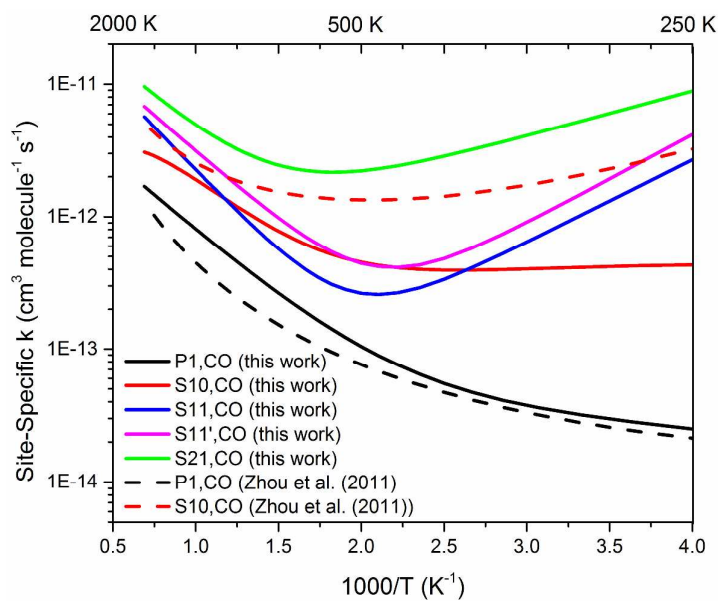


Fig. 13. Arrhenius plot of the various site-specific rate constants for the temperature range of 250 – 1450 K.

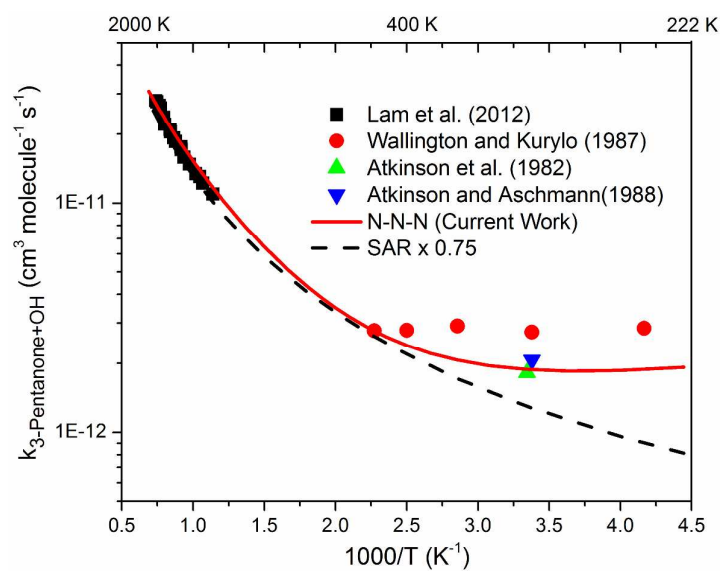


Fig. 14. Arrhenius plot of 3-pentanone + OH \rightarrow Products for the temperature range of 240 – 1353 K.

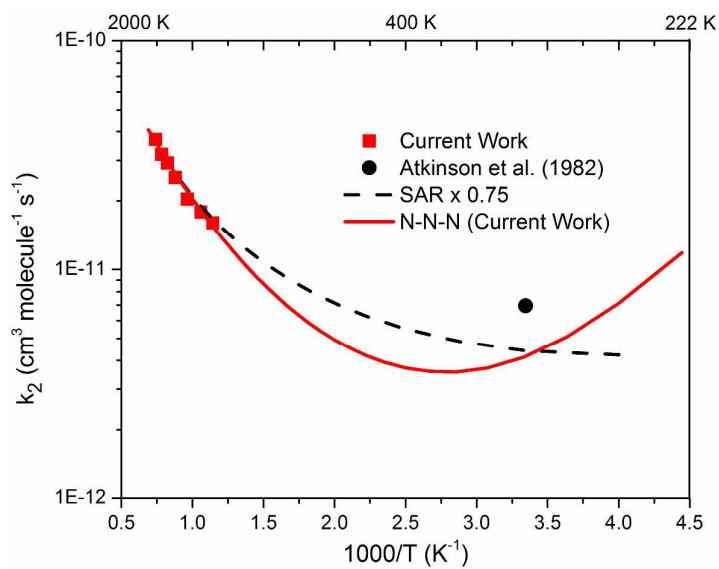


Fig. 15. Arrhenius plot of 3-hexanone + OH \rightarrow Products for the temperature range of 299 – 1350 K.

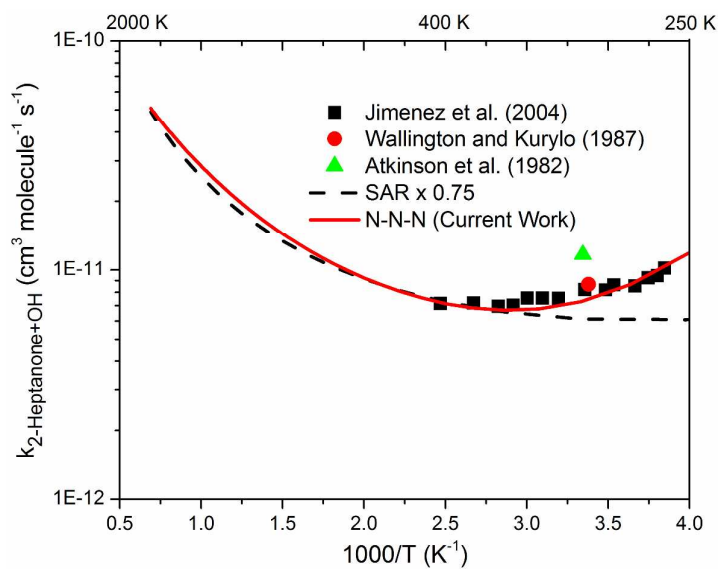


Fig. 16. Arrhenius plot of 2-heptanone + OH \rightarrow Products for the temperature range of 260 – 1450 K.

Reaction Rate Constants of H-Abstraction by OH from Large ketones:

Measurements and Site-Specific Rate Rules

Jihad Badra, Ahmed Elwardany, Aamir Farooq

Supplementary Material: Tables S1-S4

Table S1: Sub-mechanism for 2-hexanone.

Reaction	Pre-exponential Factor (A) (cm, mol, s)	Temperature exponent (B)	Activation energy (cal/mol)
$C_4H_9COCH_3 + OH \rightleftharpoons C_2H_4 + CH_2CH_2COCH_3 + H_2O$	5.280E+09	0.97	1590
$C_4H_9COCH_3 + OH \rightleftharpoons C_3H_6 + CH_3COCH_2 + H_2O$	4.68E+07	1.61	-35
$C_4H_9COCH_3 + OH \rightleftharpoons C_4H_8-1 + CH_3CO + H_2O$	4.68E+07	1.61	-35
$C_4H_9COCH_3 + OH \rightleftharpoons C_3H_7CHCO + CH_3 + H_2O$	1.146E+11	0.51	63
$C_4H_9COCH_3 + OH \rightleftharpoons PC_4H_9 + CH_2CO + H_2O$	5.100E+11	0.00	1192
$C_3H_7CHCO + OH \rightleftharpoons PC_4H_9 + CO_2$	3.730E+12	0.00	-1010
$C_3H_7CHCO + H \rightleftharpoons PC_4H_9 + CO$	4.400E+12	0.00	1459
$C_3H_7CHCO + O \rightleftharpoons C_4H_8-1 + CO_2$	3.200E+12	0.00	-437

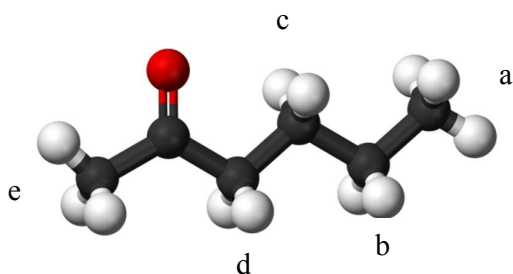


Table S2: Sub-mechanism for 3-hexanone.

Reaction	Pre-exponential Factor (A) (cm, mol, s)	Temperature exponent (B)	Activation energy (cal/mol)
$\text{C}_3\text{H}_7\text{COC}_2\text{H}_5 + \text{OH} \rightleftharpoons \text{C}_2\text{H}_4 + \text{C}_2\text{H}_5\text{COCH}_2 + \text{H}_2\text{O}$	5.280E+09	0.97	1590
$\text{C}_3\text{H}_7\text{COC}_2\text{H}_5 + \text{OH} \rightleftharpoons \text{C}_3\text{H}_6 + \text{C}_2\text{H}_5\text{CO} + \text{H}_2\text{O}$	4.680E+7	1.61	-35
$\text{C}_3\text{H}_7\text{COC}_2\text{H}_5 + \text{OH} \rightleftharpoons \text{C}_2\text{H}_5\text{CHCO} + \text{C}_2\text{H}_5 + \text{H}_2\text{O}$	1.146E+11	0.51	63
$\text{C}_3\text{H}_7\text{COC}_2\text{H}_5 + \text{OH} \rightleftharpoons \text{NC}_3\text{H}_7 + \text{CH}_3\text{CHCO} + \text{H}_2\text{O}$	5.520E+02	3.12	-1176
$\text{C}_3\text{H}_7\text{COC}_2\text{H}_5 + \text{OH} \rightleftharpoons \text{NC}_3\text{H}_7\text{CO} + \text{C}_2\text{H}_4 + \text{H}_2\text{O}$	5.280E+09	0.97	1590

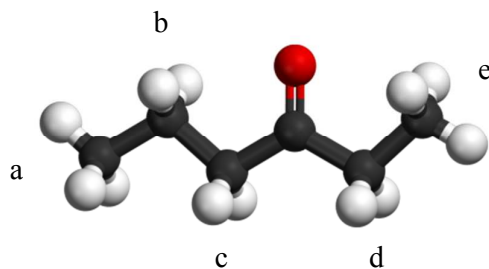


Table S3: Sub-mechanism for 3-methyl-2-pentanone.

Reaction	Pre-exponential Factor (A) (cm, mol, s)	Temperature exponent (B)	Activation energy (cal/mol)
$C_4H_9COCH_3-3 + OH \rightleftharpoons C_2H_4 + CH_3CHCOCH_2 + H_2O$	5.280E+09	0.97	1590
$C_4H_9COCH_3-3 + OH \rightleftharpoons C_4H_8 + CH_3CO + H_2O$	4.680E+7	1.61	-35
$C_4H_9COCH_3-3 + OH \rightleftharpoons C_4H_8 + CH_3CO + H_2O$	5.730e+10	0.51	63
$C_4H_9COCH_3-3 + OH \rightleftharpoons C_3H_7CHCO + CH_3 + H_2O$	5.280E+09	0.97	1590
$C_4H_9COCH_3-3 + OH \rightleftharpoons PC_4H_9 + CH_2CO + H_2O$	5.100E+11	0.00	1192
$C_3H_7CHCO + OH \rightleftharpoons PC_4H_9 + CO_2$	3.730E+12	0.00	-1010
$C_3H_7CHCO + H \rightleftharpoons PC_4H_9 + CO$	4.400E+12	0.00	1459
$C_3H_7CHCO + O \rightleftharpoons C_4H_8-1 + CO_2$	3.200E+12	0.00	-437

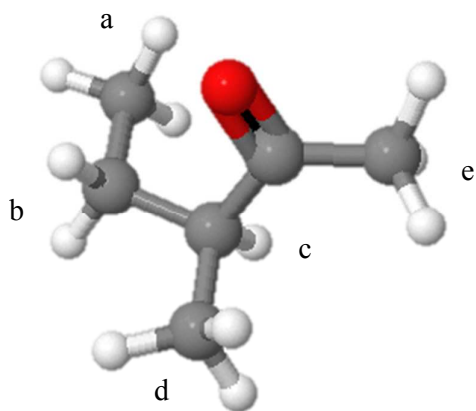


Table S4: Sub-mechanism for 4-methyl-2-pentanone.

Reaction	Pre-exponential Factor (A) (cm ³ mol ⁻¹ s ⁻¹)	Temperature exponent (B)	Activation energy (cal/mol)
$C_4H_9COCH_3-4 + OH \rightleftharpoons C_3H_6 + CH_3COCH_2 + H_2O$	1.056e+10	0.97	1590
$C_4H_9COCH_3-4 + OH \rightleftharpoons C_4H_8 + CH_3CO + H_2O$	5.730E+10	0.51	63
$C_4H_9COCH_3-4 + OH \rightleftharpoons C_3H_7CHCO + CH_3 + H_2O$	1.146E+11	0.51	63
$C_4H_9COCH_3-4 + OH \rightleftharpoons PC_4H_9 + CH_2CO + H_2O$	5.100E+11	0.00	1192
$C_3H_7CHCO + OH \rightleftharpoons PC_4H_9 + CO_2$	3.730E+12	0.00	-1010
$C_3H_7CHCO + H \rightleftharpoons PC_4H_9 + CO$	4.400E+12	0.00	1459
$C_3H_7CHCO + O \rightleftharpoons C_4H_8-1 + CO_2$	3.200E+12	0.00	-437

